ABSTRACT

Title of Thesis: FULL BLADE DIGITAL IMAGE CORRELATION (DIC) TEST APPARATUS

Andrew Collar
Master of Science, 2022

Thesis Directed by: Professor Olivier A Bauchau
Department of Aerospace Engineering

The objective of this study was to design a Digital Image Correlation (DIC) apparatus capable of measuring sectional stiffness properties of full scale helicopter blades within preexisting facilities. To do so, this study expanded on previous studies findings that deemed DIC apparatus as an ideal system to measure the strain field over composite blades. To determine the ideal apparatus to measure the sectional stiffness properties of full scale blades that can be used at facilities such as Fort Eustis in Newport News, VA., two initial concepts -the gantry and stationary system- were investigated. The study used analytical matrices like the Pugh's matrix to down select to an ideal apparatus. The study determined the ideal design through cost, distance from the blade, and accuracy to finalize a potential solution. This study identified the stationary system as the ideal system for this purpose. The proposed solution would have an initial cost of $100,000 to acquire the required equipment proposed in the current study. Through empirical and analytical methods, the solution would be able to measure the strain field within 1%.

Full Blade Digital Image Correlation (DIC) Test Apparatus

by

Andrew Nathan Collar

Thesis submitted to the Faculty of the Graduate School of the
University of Maryland, College Park in partial fulfillment
of the requirements for the degree of
Master of Science
2022

Advisory Committee:
Dr. Olivier A. Bauchau, Chair/Advisor
Dr. Sung W Lee
Dr. Vengalatorre T Nagaraj

Dedication

To my wife Dr. Niloofar Agah for all the love, support and help she provided.

Acknowledgments

I owe this gratitude to all the people that supported me and my efforts in my research and graduate efforts. With out their love and support I would have not been able or had the strength to complete my graduate degree.

Firstly, I would like to thank my advisor Professor Olivier A Bauchau for giving me the opportunity to work on a highly desirable research project. His guidance and knowledge were instrumental in my ability to complete the research. Dr. Bauchau always had an open door policy to answer question and provide sound feedback into the research. I appreciate all the effort he gave to helping complete this study.

I want to next, thank the members of my committee, Dr. Nagaraj and Dr. Lee for their time and input on the study. Their guidance and comments helped refine the information within the study.

I want to thank all of my friends and classmates for all their help and support. They made this 3-year journey an enjoyable ride. Without their constant support and motivation, I would have never been able to accomplish this endeavor.

To my supervisor, co-workers, and mentor at NAVAIR, I especially thank you. Your flexibility, guidance, and support allowed me to accomplish one of my goals. I will never forget the support you gave to me.

Finally, I want to thank my wife Dr. Niloofar Agah, my stepson Saam Daei, and the rest of my family for all the love and support given during this time. Your commitment, understanding, and patience helped provide the environment for me to succeed in completing the study. Your confidence in my ability was the motivation I needed.

Table of Contents

List of Tables

List of Figures

Chapter 1: Introduction

Chapter 1 provides the motivation for this thesis to measure sectional stiffness properties of helicopter blades. This chapter reviews studies conducted on using Digital Image Correlation (DIC), measuring strain on composite helicopter blades and airframes. It also identifies a potential facility having the required loading cell.

1.1 Motivation

The objective of this thesis is to create a DIC apparatus capable of measuring sectional stiffness properties of full scale helicopter blades within preexisting facilities. This study recognizes that the design of current blades utilize light weight composite materials and complex geometric designs to maintain structural integrity, while maximizing performance. These designs are studied using the latest analytical tools, that couple the aerodynamics with the structural dynamics, to calculate the aeromechanic properties of the rotor blade. Moreover, these designs require a new set of devices to accurately measure the sectional stiffness properties of these new blades. This thesis does not intend to go into details of the analytical tools and devices, since in the study ”A Strain-Based Experimental Methodology for Measuring Sectional Stiffness Properties of Composite Blades” by Tyler Sinotte (2020) this topic has already been explored in detail. Sinotte

(2020) identified that the previous analytical tools, such as Finite Element Analysis (FEA) and Computational Fluid Dynamics (CFD), failed to accurately predict the aeromechanic properties of rotorcraft. He concluded that obtaining the sectional stiffness properties, for blades of arbitrary configuration made of anisotropic materials, can be quite daunting. In many cases, adjustments are made to correlate the predicted sectional stiffness properties against the measured. In recent years, newer robust analytical tools, such as *Dymore*, CAMRAD II, RCAS, and UMARC, use finite element beam theory for anisotropic materials and flexible multibody dynamics to predict the sectional stiffness matrix. [7]

Furthermore, Sinotte (2020) reviewed previous measurement techniques to determine their effectiveness in measuring the full six by six sectional stiffness matrix. Techniques, such as rotational based measurements, deflection based measurements, and frequency based measurements, were able to measure specific entries of the sectional stiffness matrix, but failed to measure the full six by six sectional stiffness matrix. Other techniques, like strain gauges, distributed wire sensors, and distributed strain sensors, use contact based strain measurements to determine the sectional stiffness properties. These techniques provided the ability to calculate the full six by six sectional stiffness matrix; on the other side, they were expensive and required an extensive network to measure span wise variations. Sinotte (2020) concluded that for a full scale helicopter blade, a non-contact based strain measurement would be the ideal apparatus to measure the six by six sectional stiffness matrix. He reviewed three types of non-contact strain measurement devices: electronic speckle pattern interferometry (ESPI), projection Moiré interferometry (PMI), and DIC. According to his study, DIC would be the ideal system since it provides a good tradeoff between cost and accuracy of measurements. [7]

Sinotte (2020) further concluded that DIC was able to measure the sectional stiffness properties of composite blades. The data reduction process could calculate the off-diagonal components of the sectional compliance matrix. DIC could measure spanwise variations in properties. The study identified DIC requiring large strains to accurately measure the sectional stiffness properties of composite materials. This issue was raised due to the inability for the 6-axis load cell to apply significant loading in the axial direction. In other cases, such as torsion and bending moments, DIC correlated well to the predicted values. This confirmed that the limitation was with the 6-axis load cell and not with DIC. [7]

This study intends to build upon Sinotte's (2020) conclusion of requiring non-destructive loads that produce strains far greater than 50 $\mu\epsilon$. It should be noted that the lower limit of DIC is 20-50 $\mu\epsilon$, depending on the hardware used. To serve this purpose, this thesis plans to identify facilities that have the load cells with the capability to produce flight loads. Moreover, this thesis plans to review other DIC studies to determine the effectiveness of DIC to measure strain on full scale structures. Lastly, this study determines the type of DIC apparatus, the specific design, estimating the associated cost, the relative accuracy, and drafts the initial procedures for operation.

1.2 DIC and Available Load Cell

1.2.1 NASA DIC Apparatus

Initially, the researcher reviewed studies that utilized DIC to measured strain on aircraft structures. Between 2013 and 2015, NASA conducted a series of tests for full-scale crash tests at the Landing and Impact Research Facility (LandIR) at NASA Langley Research Center (LaRC). These test incorporated The Rotorcraft Airframe Crash Testbed (TRACT) where two CH-46E airframes were dropped from a predetermined height to study the impact on the airframe as well as test dummies situated within the cabin. The other test was the Emergency Locator Transmitter Survivability and Reliability (ELTSAR) project, where three Cessna 172 were dropped from a predetermined height and location to simulate a Control Flight Into Terrain (CFIT) and study the impact on the airframe. [1,2]

During both of these tests, NASA implemented a DIC apparatus with two high speed cameras situated at different calculated distances away from the crash bed. These different distances allowed for high speed cameras to reliably capture the crash in real time while reducing the risk of damaging the cameras. Then NASA analyzed all of the footage and calculated relevant strains from DIC. Figures 1.1 provides the location of the cameras relative to the ELTSAR experiment, considering the cameras were positioned far enough from the intended test area to capture the entire crash. Figure 1.2 provides the post analysis for the TRACT experiment. According to this study, the DIC Apparatus was able to precisely measure the strain during the entire crash. [1,2] Thus, the researcher concluded that DIC is an effective measuring device for full scale aircraft structures.

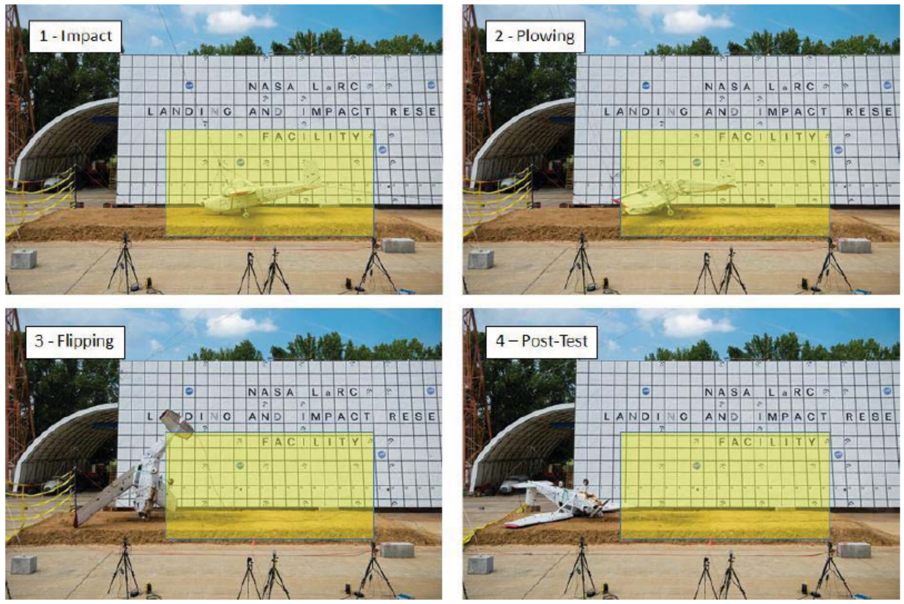

Figure 1.1: NASA ELTSAR experiment with the location of the cameras relative to the crash site. [1]

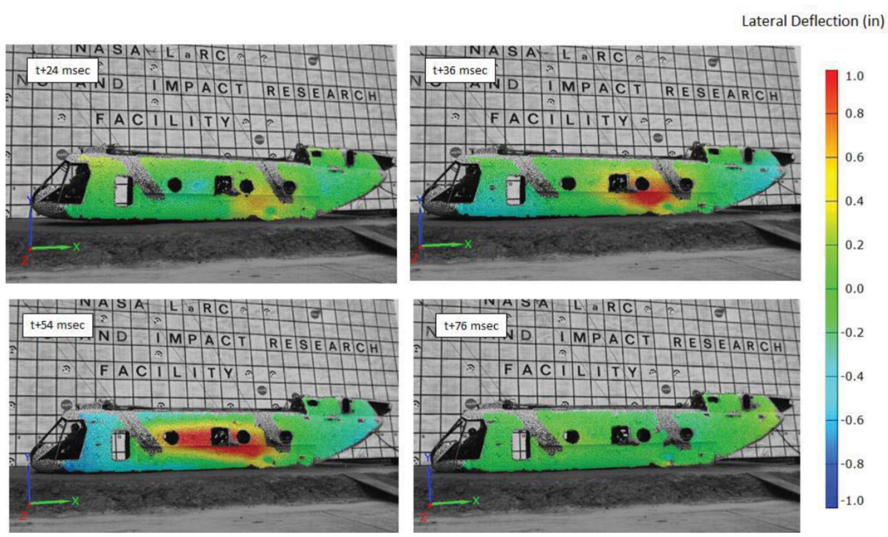

Figure 1.2: NASA TRACT post analysis of the strain from a 30 ft drop. [2]

This research identified potential calibration methods for full scale structures. Due to the positioning of the cameras and the size of the aircraft tested, NASA had to use a different solution to calibrate the apparatus. Prior to each test, NASA had designed a calibration grid shown in Figures 1.1 and 1.2 as a white panel behind the crashing aircraft.

To calibrate the cameras, the team would tow the aircraft across the grid. [1, 2]

An issue noted in the study was the location of the cameras. During the ELTSAR experiment, the testers miscalculated the location of both cameras. They assumed that the crash would remain within the designated area and not continue outside the field of view of the cameras. When the actual crash commenced, the aircraft nose tire dug into the ground and the momentum caused the aircraft to flip over the nose of the aircraft. This caused parts of the crash to happen outside the field of view of the cameras losing critical data. Again, this is shown in figure 1.1 with the aircraft impacting, plowing, flipping, and finally resting on the upper wing outside the cameras field of view. [1] Hence this matter was taken into consideration in the current study.

1.2.2 Fort Eustis Load Cell

After reviewing the effectiveness of DIC, the researcher identified Fort Eustis in Newport News, VA as a potential facility where they had conducted blade tests in the past. Moreover, the researcher reached out to Fort Eustis to inquire about their blade load test cell. As shown in figure 1.3, the facility has a 4-axis blade loading apparatus.

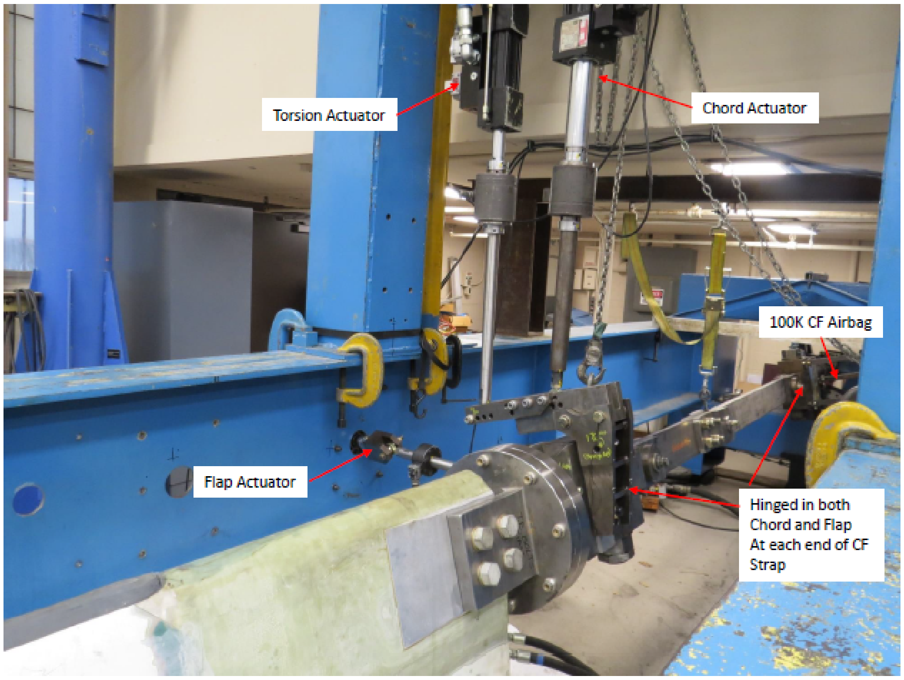

Figure 1.3: The blade load apparatus at Fort Eustis, Norfolk, Va. [3]

The apparatus is capable of applying 100 kips of CF, 5 to 20 kips in the flap direction, and 1 to 10 kips of torsion. [3] Thus, the facility has the capability to apply the loads necessary for DIC.

Chapter 2: Initial Concepts

Chapter 2 develops the initial concepts based on the research discussed in chapter 1. Moreover, it provides the requirements and design drivers applied to determine the ideal system. This chapter analytically evaluates the requirements and design drivers to determine the ideal initial concepts to down select to a single design.

2.1 Requirements and Design Drivers

Two different preliminary designs suggested possible solutions to map the strains across a full blade: a stationary design with multiple pairs of cameras focused on certain sections of the blade and a gantry system, in which two cameras translate down the blade to map the strain. To evaluate the designs an initial set of requirements had to be defined. These requirements focused on a system that needed to be implemented within a preexisting facility with a load test capable of producing flight loads, high accuracy, and easily configurable to test any blade. To conduct an accurate test, the following requirements were taken into consideration:

- The DIC apparatus shall be designed to work within a preexisting facility with minimal reconfiguration.

- The system shall have an accuracy to measure strain within 1%.
- The system shall be able to capture the entire helicopter blade regardless of length or type.

From these initial requirements, the following set of design drivers were developed:

- Cost - minimum cost system that achieves the required accuracy
- Complexity - easy to design and implement within existing facilities.
- Ease of Use - intuitive system that requires minimum training for the operator to be proficient in the use of the device.
- Integrable - a system that can integrate with the current facility layout.
- Timeliness - system that minimizes both data capture and calibration times.
- Accuracy - system that provides the maximum accuracy to measure the strain.
- Reconfigurable - a system that requires minimum reconfiguration to be implemented on other blades.

In order to evaluate the proposed designed solution, an Analytical Hierarchy Process (AHP) was designed to rank these drivers from 1/5-5 to determine the desirability for each. Table 2.1 provides the results to the AHP:

Table 2.1: AHP Matrix

	Cost	Complexity	Integrable	Ease of Use	Timeliness	Accuracy	Reconfigurable	Priority Vector (%)
Cost	1	1	2	4	5	1/2	3	19.7
Complexity	1	1	2	4	5	1/2	3	19.7
Integrable	1/2	1/2	1	3	4	1/3	2	12.3
Ease of Use	1/4	1/4	1/3	1	2	1/5	1/2	5.20
Timeliness	1/5	1/5	1/4	1/2	1	1/5	1/3	3.70
Accuracy	2	2	3	5	5	1	4	31.7
Reconfigurable	1/3	1/3	1/2	2	3	1/4	1	8.00

It was determined that accuracy received the highest percentage weight with a priority of 31.7% since the measuring device needed to reliably and accurately capture data. Next major design drivers were cost and complexity with a priority of 19.7%. Integrable and Reconfigurable drivers followed as the DIC is required to operate in existing facilities and to capture strains on all existing blades. The least important design drivers are ease of use and timeliness, which received a priority of 3% and 5%, respectively.

2.2 Concepts and Down Selection

Figure 2.1 presents the initial concept of the gantry system. As shown, the gantry crane would be stationed at a predetermined working distance and moves a pair of cameras across the blade. A software directs the cameras to photograph at fixed intervals along the blade until the entire blade is mapped. Then the software analyzes and provides the strain across the blade. In certain cases where the facility prevents the proper field of view, the setup can incorporate the ability for cameras to move chordwise as well as spanwise.

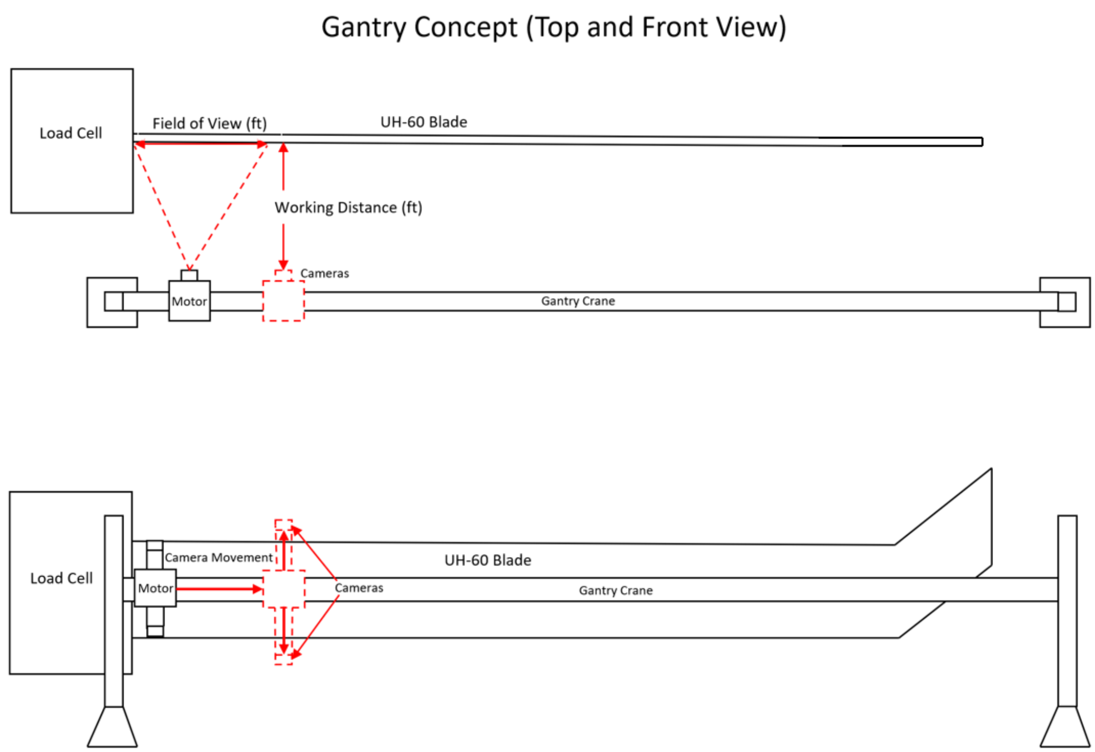

Figure 2.1: An initial concept for the gantry system. As depicted there will be a pair of cameras attached to a motor that will translate along the blade. In certain cases, the cameras will be able to move up and down to map the chordwise strain. The cameras will take a portion of the blade called the field of view based on the position of the gantry system called the working distance.

Figure 2.2 presents the concept of the stationary system. As depicted, each pair of cameras is positioned at a distance from the blade so the entire blade is photographed. Each pair of cameras will capture a portion of the blade called the field of view. The number of the pairs of the cameras determines the working distance as indicated in figure 2.2. Then once again the software uses the images from the multiple cameras to evaluate the strain across the blade. The minimum working distance for the cameras is limited by the chord length, since each pair of cameras will need to have a field of view of the entire chord.

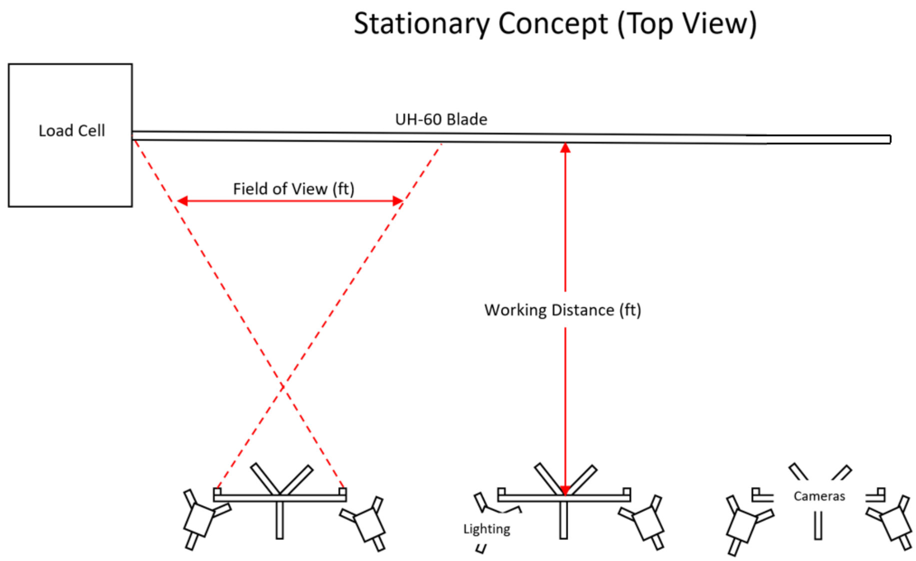

Figure 2.2: An initial concept for the stationary system. As depicted there will be a number of pairs of cameras positioned at a defined working distance, how far the cameras are from the blade. Each pair of cameras will capture a portion of the blade also known as the field of view. Lights will be positioned near the cameras to provide sufficient lighting.

To determine the best solution, a Pugh's Matrix evaluated the proposed designs against the design drivers. A -4 to 4 scale assessed each design against the design drivers with the stationary system being the baseline at 0. A negative value represents a limitation while a positive value represents an advantage of gantry to stationary system. Tables 2.2 provides the final results for the Pugh Matrix.

Table 2.2: Pugh Matrix

	Weight	Stationary	Gantry
Cost	0.197	0	-3
Complexity	0.197	0	-3
Integrable	0.123	0	3
ease of use	0.052	0	-2
Timely	0.037	0	-2
Accuracy	0.317	0	-2
Reconfigurable	0.080	0	3
Score		0	-1.38

A pros and cons table 2.3 showed below was developed to expand on each design driver and proposed solution.

Table 2.3: Stationary vs Gantry Pros and Cons

Stationary	**Gantry**
Pros: • Cheap due to only requiring cameras, lenses and simple software to operate. • Design requiring only cameras, lenses, tripods and simplistic software to operate. • Easy to use and needing minimal training to be proficient in capturing and analyzing data. • Quick since all cameras will simultaneously take photo of the blade and minimal calibrations. • Failure of a pair of cameras does not prevent system from measuring strain. • High accuracy since cameras remain fixed and only need one calibration.	**Cons:** • Expensive due to complexity of the system. • Complex design requiring motors, wiring, and other features to move and stabilize cameras. A rigorous software to operate system and accurately take pictures of entire span wise blade. • Difficult to operate and needing robust training to operate the system. • Slow since system will have to take a single picture and move to the next position. The system will require multiple calibrations during this process as well. • If a single camera fails system will be unable to measure strain. • Low accuracy since cameras move and focus will adjust needing multiple calibrations to remain accurate.

Cons:	Pros:
• Impractical for confined spaces and large helicopter blades. • Dependent on facility layout and unusable if test cell prevents proper view of blade. • Major adjustments and number of cameras needed to capture different lengths of blades. • Lighting dependent which will reduce accuracy if lighting unavailable.	• Ideal for confined spaces since cameras can be moved both span wise and chord wise to take picture of the blade. • independent on facility layout. • Minimal adjustments needed to capture different lengths of blades. • Minimal lighting to accurately capture strain due to the ability for the gantry to be closer to the blade.

The accuracy value from table 2.2 was based on the information given by Correlated Solutions. Correlated Solution states that moving the cameras will shift the focus either due to moving the cameras closer or further away from the specimen or causing the lens to shift from the current setting. Figure 2.3 shows how shifting focus reduces accuracy. The black curve provides the ideal focus, while the red curve simulates a poorly focused lens. According to Correlated Solutions, the software maps the dot pattern on the specimen. Then it creates unique identifiers for the specific dots that will be tracked. A narrow and large trough, like that shown in figure 2.3, allows the software to ignore dots that are not associated with the mapped dots. Thus for an ideal setup, a high error, as shown by the black curve, is necessary for the software to remove outlying dots and accurately track the specific mapped dots. Inversely, the unfocused camera, represented as the red curve in figure 2.3, fails to provide the required resolution for the software to distinguish the mapped dots. This low error causes the software to misinterpret the specific mapped dots and to start tracking incorrect dots. [4]

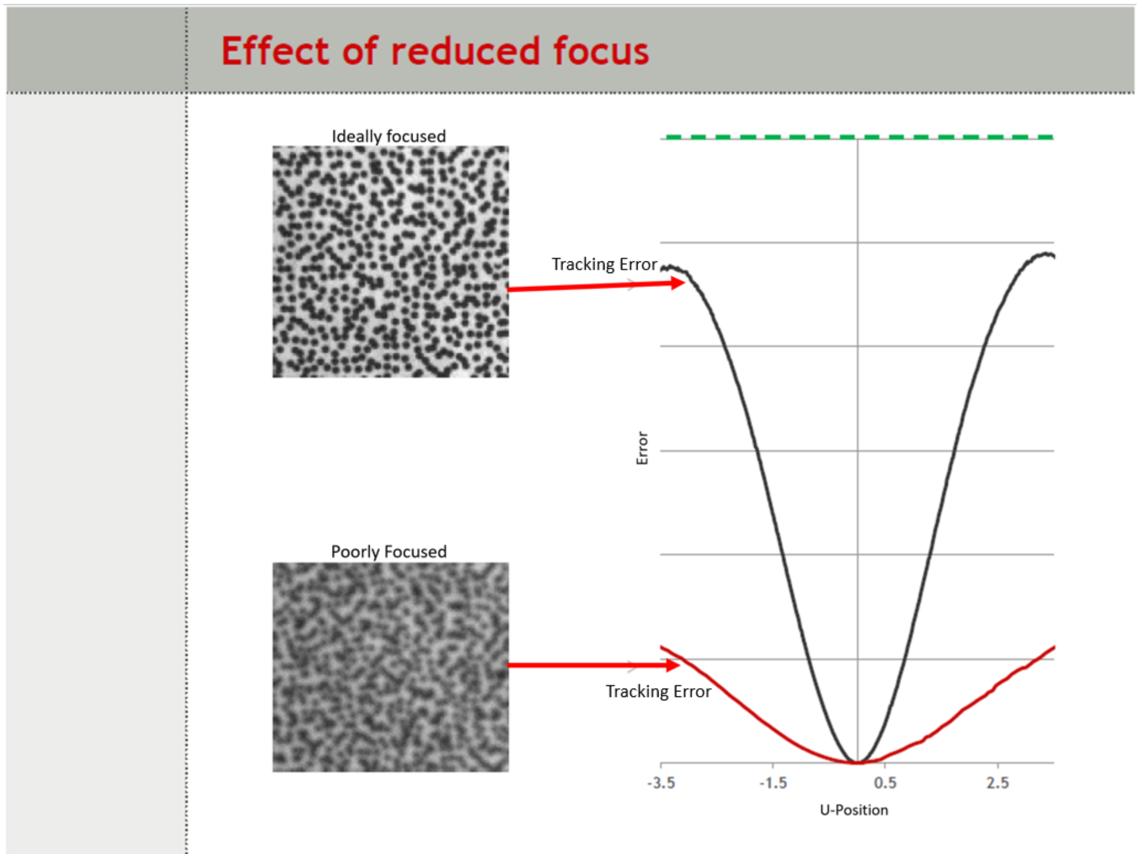

Figure 2.3: The effects of focus on the noise of the cameras. The black curve represents the ideal focus and has the least amount of noise with a large narrow trough. The high error is required for the software to correctly track the associated dot. The red curve represents poor focus and has a significant amount of noise with a small wide trough. This is also shown with low amounts of error, since the software is unable to track the correct dot. The x-axis is the horizontal position of pixels and the associated dot. The y-axis is the error due to the software identifying the parameters of a dot against the parameters passed during the mapping phase. [4]

This becomes a limitation to the gantry system, since the movement of the system will cause the lens to shift and reduce accuracy. The shifting of the lens causes another problem: the gantry system will require re-calibration periodically, during each test, to maintain accuracy. Now the software will need to incorporate a calibration parameter, thus increasing the total time for data capture and the complexity of the software adding another limitation. Inversely, lighting becomes an issue for the stationary system. If the required distance causes insufficient lighting then it will result in lower accuracy. Figure 2.4 illustrates this effect of insufficient lighting. The accuracy would shift from the black (ideal) curve to the red (poorer) curve. As stated before, the software requires a large narrow trough to accurately track the associated dot. This large narrow trough produces a high error which allows the software to ignore dots not associated to the mapped dots. A wide small trough, like the one depicted in figure 2.4, prevents the software from accurately tracking the associated dot. Again, this small wide trough produces low error which causes the software to track incorrect dots. From the information provided, the gantry system received a -2 because there is a higher probability that the lenses will shift out of focus, versus the stationary system having insufficient lighting. The same process was conducted on the remaining design drivers to calculate relative advantage of each design.

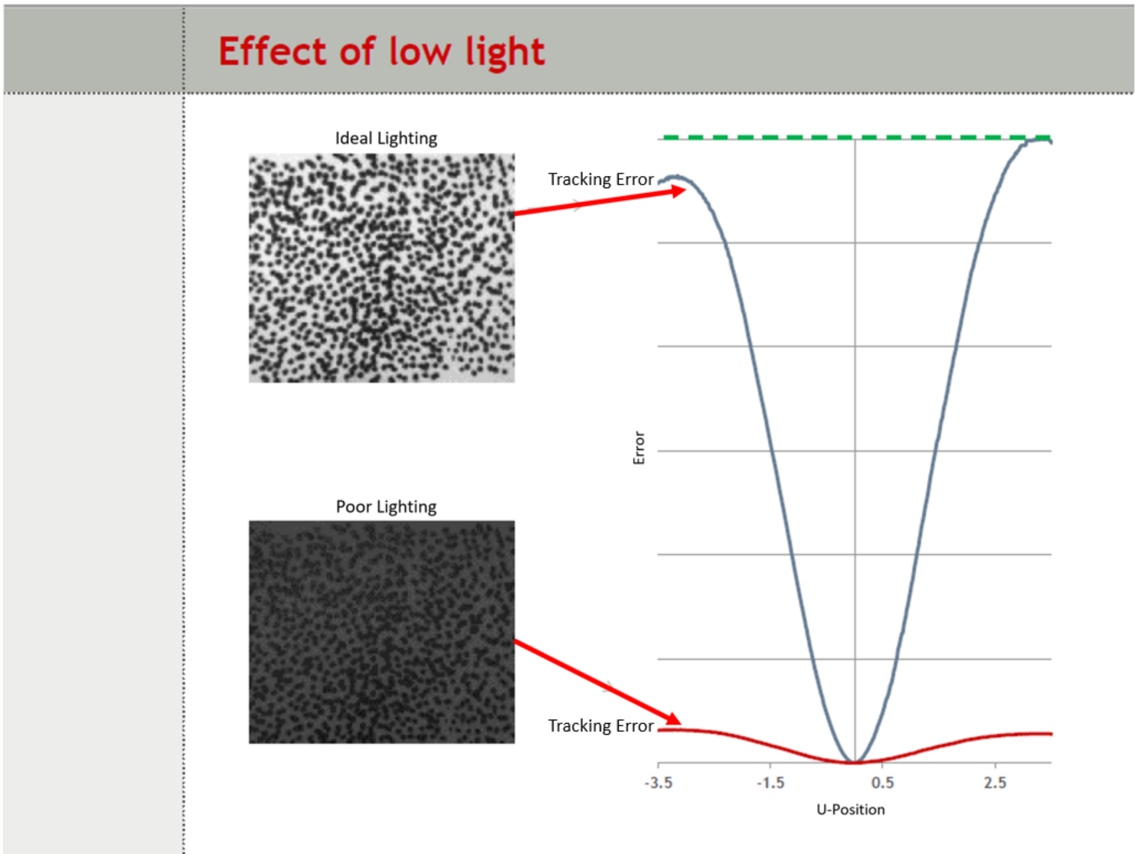

Figure 2.4: The effects of lighting on the noise of the cameras. The black curve represents the ideal lighting and has the least amount of noise with a large narrow trough. The high error is required for the software to correctly track the associated dot. The red curve represents poor lighting and has a significant amount of noise with a small wide trough. This is also shown with low amounts of error, since the software is unable to track the correct dot. The x-axis is the horizontal position of pixels and the associated dot. The y-axis is the error of the software tracking the associated dot. The y-axis is the error due to the software identifying the parameters of a dot against the parameters passed during the mapping phase. [4]

2.3 Initial Proposed Solution

Using tables 2.2 and 2.3, the stationary system was determined to be the ideal apparatus in the current study. The accuracy, cost, and complexity drove the decision to design a stationary system. Table 2.2 shows the stationary system outscored the gantry system in these critical design drivers. As for accuracy, the stationary system reliably maintained the required accuracy in comparison to the gantry system. For the cost and complexity, the stationary system would be comparably cheaper and easier to design and implement within existing facilities than the gantry system. Although gantry system is more integrable and reconfigurable, the weight of those design drivers were deemed unimportant compared to cost, complexity, and accuracy.

Chapter 3: Designing Ideal Stationary Apparatus

Chapter 3 develops the ideal set of stationary systems using analytical tools and experiment. This chapter covers the process in determining the best camera and lens for the solution by gathering information on the specification for different cameras and lenses. Using equations for working distance and cost to identify the initial set of number of cameras, this chapter refines the number of cameras required for the study based on experimentation to asses the accuracy of each solution. Lastly, it identifies the set of ideal solutions based on cost, accuracy, and distance to the specimen.

3.1 Number of Cameras versus Cost

The stationary system, as described in section 2.2, uses a number of pairs of cameras to capture the strain field over the entire blade. The number of pairs of cameras is dependent on the type of cameras, the dimensions of the blade, the size of the facility, and the smallest feature on the blade. To determine the type of camera the researcher reached out to Correlated Solutions, a company that provides DIC equipment, and they provided 2 types of cameras: 5 MP and 12 MP. Correlated Solution suggested the 12 MP to maximize accuracy, since there are more available pixels compared to the 5 MP. Then the researcher decided the type of lens required for the application. Correlated Solution provided 3 different lenses: 8 mm, 20 mm, and 50 mm. Again, they suggested using the 20 mm and 50 mm to minimize distortions, which increases accuracy. The researcher used Correlated Solutions estimated working distance (WD) for a single pair of cameras with a 3 ft x 26.5 ft specimen, which was 41 ft WD for 20 mm and 103 ft WD for the 50 mm, to determine the ideal lens. This finalized the camera choice to a 12 MP camera with 20 mm lens due to the high accuracy versus the relative distance.

Equation 3.1 calculates the required working distance based on a specified field of view. Where *SS* is the sensor size for the camera, *FOV* is the field of view for the camera, *WD* the working distance, and *f* the focal length for the lens.

$$WD = \frac{FOV \times f}{SS} \tag{3.1}$$

The field of view was computed by equation 3.2, where *b* is the span and *NoC* the number of cameras.

$$FOV = \frac{b}{NoC} \tag{3.2}$$

An iterative process was used to determine the field of view by setting the span to that of an UH-60 blade and increasing the number of cameras. Then the researcher applied the value into equation 3.1 along with diagonal size for sensor size from table 3.1.

Table 3.1: Sony IMX253 Specifications

Diagonal Size	17.6mm
Pixel Size	3.4μm x 3.4 μm
Resolution	4000x3096

Table 3.2 provides the working distance based on equations 3.1 and 3.2. For an UH-60 blade, the number of cameras is limited to 8, since increasing the number of cameras would prevent fully capturing the chord and require double the number of pairs of cameras. This is due to the field of view of the cameras being only able to capture 2.94 ft and not the entire chord.

Table 3.2: field of view and WD determined from the number of pair of cameras

Number of Cameras (Pairs)	Working Distance (ft)	Field of View (ft)
1	30.11	26.5
2	15.05	13.25
3	10.03	8.83
4	7.52	6.625
5	6.02	5.3
6	5.01	4.41
7	4.30	3.78
8	3.76	3.31
9	3.34	2.94
10	3.01	2.65

The best solution for the number of pairs of cameras was evaluated from the cost for each pair of cameras and lenses. Correlated Solution provided an estimate of \$6000 per pair of 12 MP cameras and \$5600 per pair of 20 mm lenses. Equation 3.3 assesses the total cost for DIC apparatus from the cost for each pair of cameras and lenses, where *NoC* is the number of pair of cameras.

$$TC = NoC \times 6000 + NoC \times 5600 \tag{3.3}$$

Table 3.3 provides the initial cost estimate based only for the cameras and lenses.

Table 3.3: Initial Cost of Stationary System

Number of Cameras (Pair)	Total Cost ($)
1	11600
2	23200
3	34800
4	46400
5	58000
6	69600
7	81200
8	92800
9	104,400
10	116,000

According to tables 3.2 and 3.3, the initial estimate for the number of pair of cameras is between 4-7. A minimum of 4 pairs of cameras is assumed to be the ideal number to accommodate most facilities. The maximum of 7 pairs of cameras was determined through figure 3.1. This figure illustrates the relationship between cost and working distance. At the beginning there is a steep curve in the working distance as cost steadily increases. After about 7 pairs of cameras, the curve begins to level out while cost still continues to steadily increase.

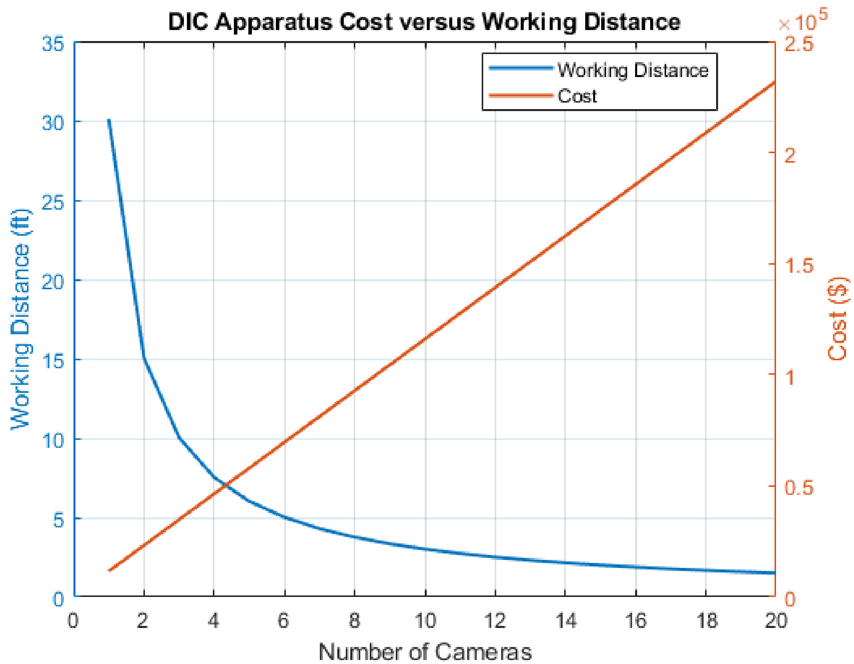

Figure 3.1: Cost of Apparatus versus the working distance from the test specimen

3.2 Number of Cameras versus Accuracy

Equations 3.1, 3.2, and 3.3 estimated the best solution to between 4-7 pairs of cameras. To further refine the selection, the researcher conducted an experiment to measure the relative accuracy for each solution. The experiment used a 6-axis test cell with load sensing unit and a pair of cameras to measure the strain. Then the researcher compared the predicted values to the measured values.

3.2.1 6-axis Load Apparatus

A 6-axis Load Apparatus shown in figure 3.2 applied the necessary loads to strain the specimen. The load apparatus works by a pulley system at the base with ropes attached to points at the top of the test specimen shown in figure 3.3.

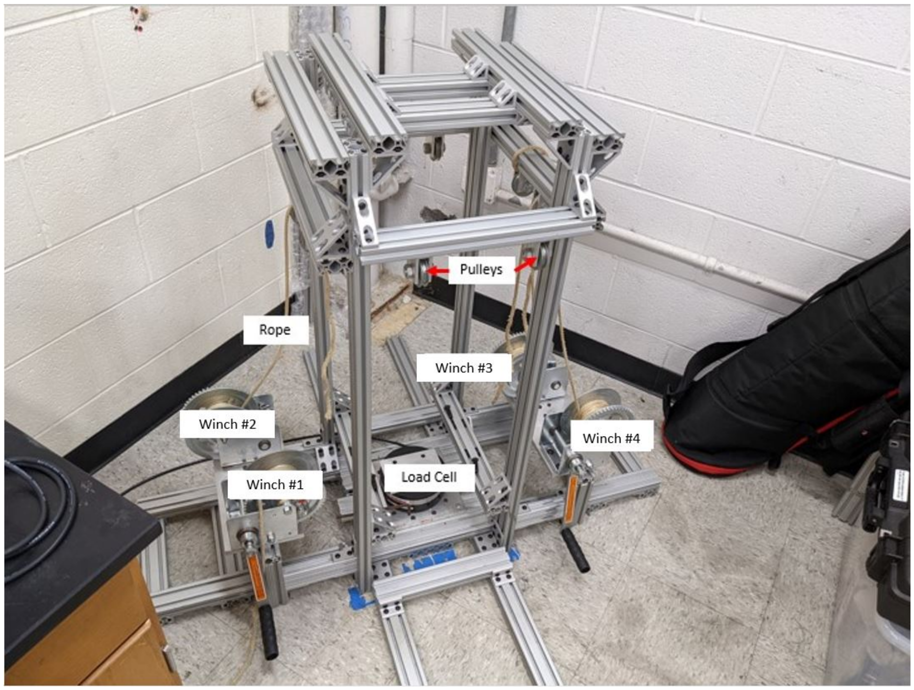

Figure 3.2: 6-Axis test apparatus used to apply loads.

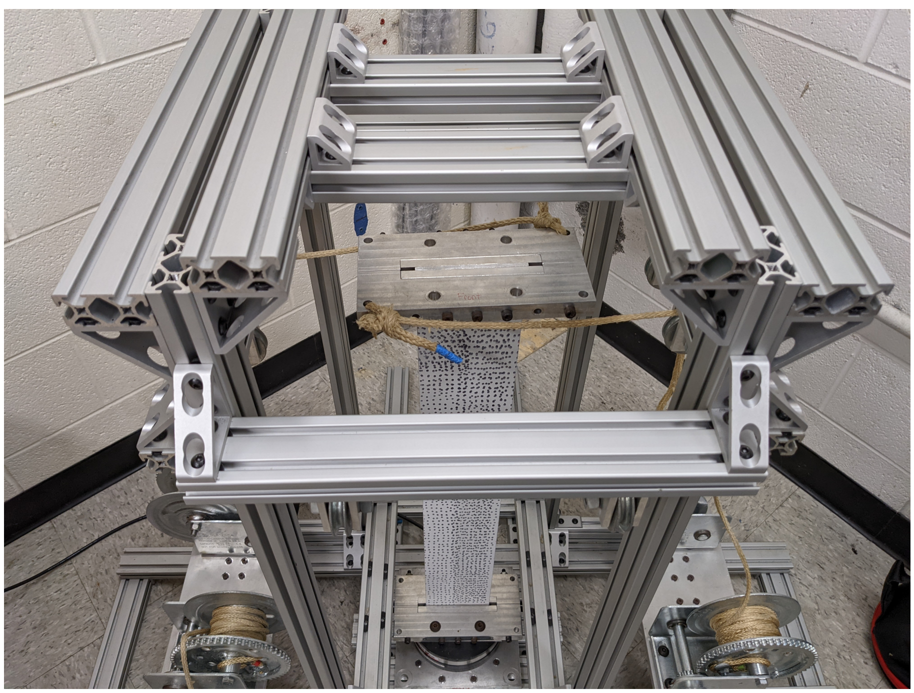

Figure 3.3: Top of Aluminum beam where the loads are applied through the ropes.

Depending on the load, certain winches would be turned to achieve the desired loading.

To accurately measure the loads, a load cell with attachments points to the specimen illustrated in figure 3.4. To apply the correct loading, only the corresponding winches would be used. For example, if an axial load required all winches will turn until the desired load achieved. For a particular bending moment, only the winches required to bend the specimen would be turned.

Figure 3.4: Aluminum Beam attached to the load cell.

3.2.2 Test Specimen

A rectangular aluminum beam served as the test specimen for all experiments. The beam was 0.3379 ft x 2.414 ft with a thickness of 0.1925 inch presented in figure 3.5. Mounting brackets attached to the base and top served as means to string the rope through and attach the base to the load cell. Dot sizes and patterns were painted on the surface to provide reference points for the software to track. Depending on the distance, different sizes and dot patterns were used. For distances of 4 ft and closer a 1/64 inch dot pattern was painted on the specimen and distances greater a 1/8 inch dot pattern was painted as shown in figures 3.5(a) and 3.5(b).

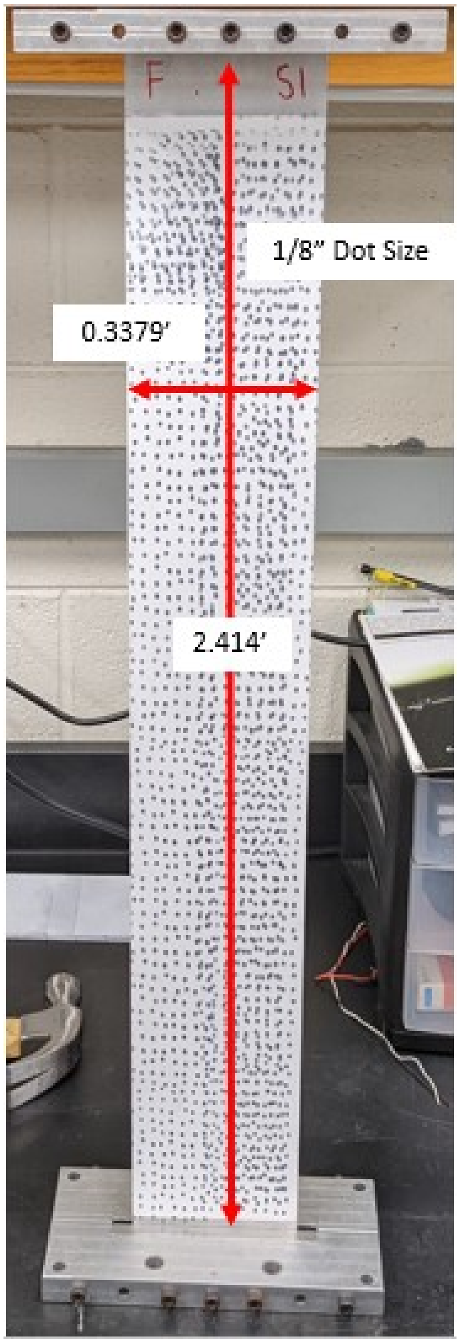

(a) Aluminum Beam with 1/8 inch dot pattern

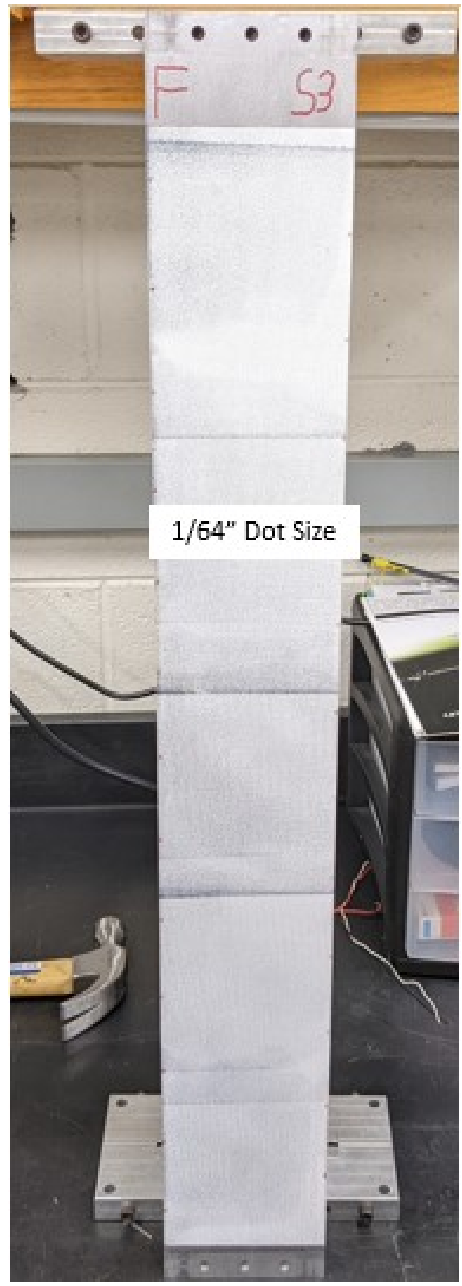

(b) Aluminum Beam with 1/64 inch dot pattern

Figure 3.5: Aluminum Beam test specimens.

3.2.3 DIC Apparatus

A pair of Correlated Solutions 5 MP cameras with 5 mm lenses set at 22 inches apart are mounted to a bracket attached to a tripod. The cameras are set to between 5° and 15° from the vertical depending on the placement of the cameras and the desired stereo angle. The stereo angle being the angle required for the cameras to capture in and out of plain displacement. The desired angle was set by focusing the cameras to the center of the specimen, which was 15° for the initial test and decreased to 5° as the working distance increased. Figures 3.6 and 3.9 illustrate the DIC Apparatus, the relative angle, and the initial test setup.

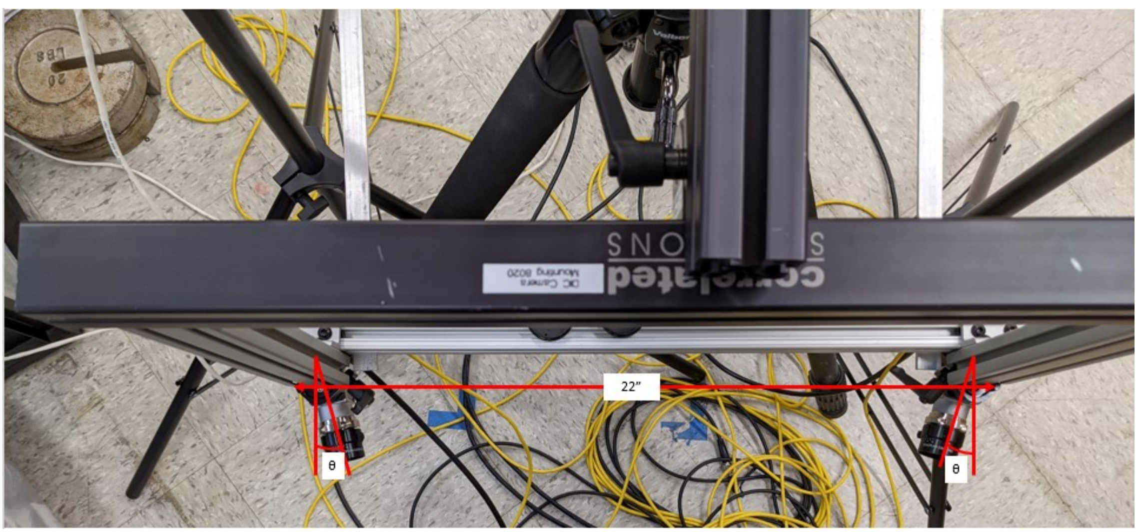

Figure 3.6: 5 MP Cameras location and angle set.

3.2.4 Lighting

Two LED DIC lighting provided the necessary luminosity for accurate measurements. The placement of the lights depended on the placement of the cameras. At closer distances, the lighting source was placed behind the DIC Apparatus. As the cameras were placed further back, the lighting source was placed closer to the test apparatus and outside the view of the cameras. Figures 3.7 and 3.9 show the type and placement of the lighting with respect to the DIC Apparatus.

Figure 3.7: DIC Lighting used to provide the necessary luminosity to accurately measure strain.

3.2.5 Data Collection Equipment

National Instruments (NI) USB-6251 and USB-6210 Data Acquisition (DAQ) shown in figure 3.8 were used to operate equipment and capture data. The NI USB-6251 collected and operated all DIC cameras while the NI USB-6210 only collected the loads.

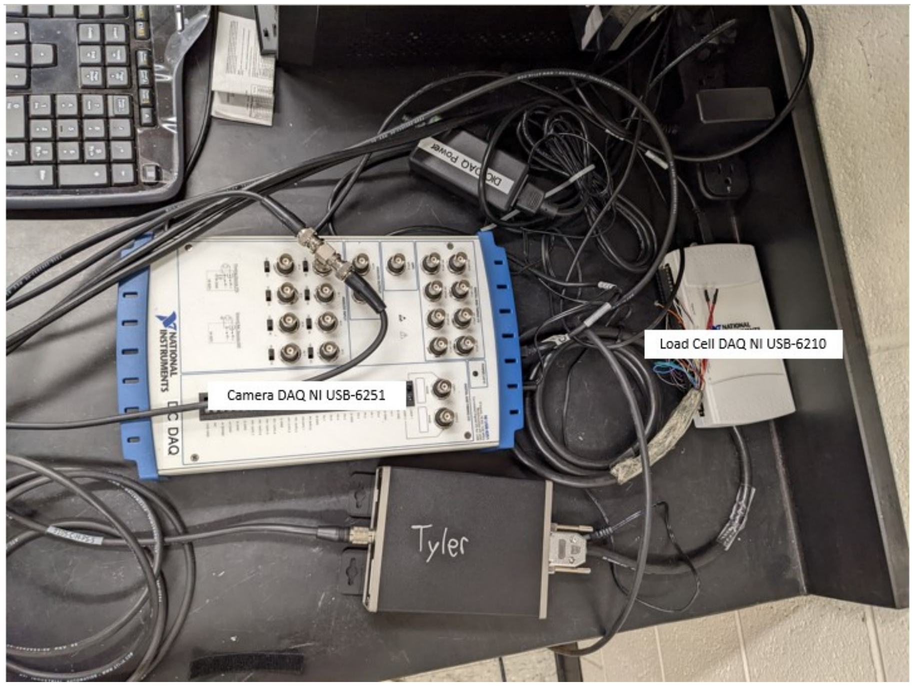

Figure 3.8: NI USB-6251 and USB-6210 DAQ used to control cameras and collect all relevant data.

3.2.6 Test Procedure

The test procedure began with the calibration of the system. The test and DIC apparatuses were setup according to figure 3.9 with the DIC apparatus being placed 3 ft from the test apparatus and the lighting right behind the cameras. The test specimen was removed during the calibration phase.

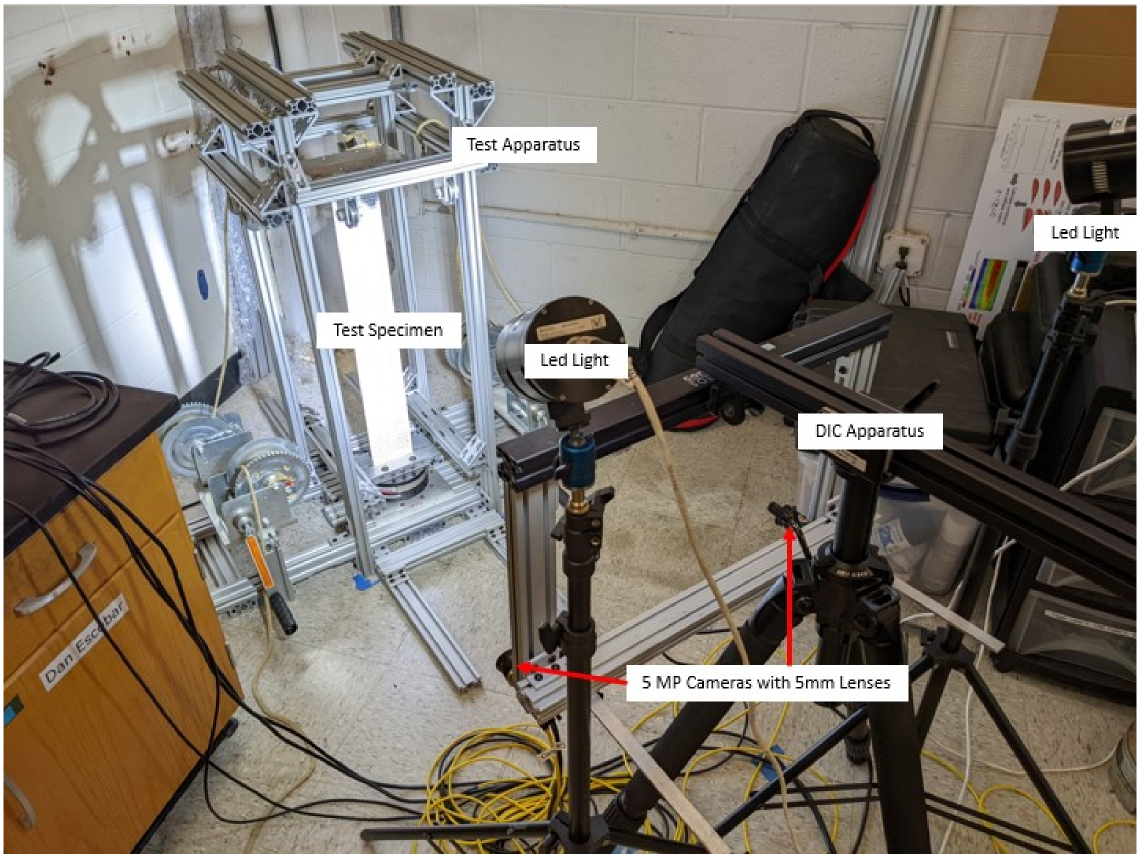

Figure 3.9: Test condition for DIC Apparatus at 3 ft.

The system was calibrated using Correlated Solutions Aluminum Calibration Sets 10 mm and 14 mm as shown in figure 3.10. For distances of 4 ft or less, the 10 mm calibration set was required to calibrate the system, while the 14 mm set was required for any distance greater. The calibration worked by taking 50 different pictures with the calibration set in different position and angles. Note for the system to be ideally calibrated Correlated Solution suggest 50 or greater number of photos. The calibration sets need to placed in different locations, orientations, angles, and distances. Lastly, for ideal calibration Correlated Solutions suggests that the calibration set be placed at the perimeter of the field of view for both cameras. [8] Once completed, the system was calibrated utilizing proprietary software. Figure 3.11 provides an ideal calibration being less than 0.1.

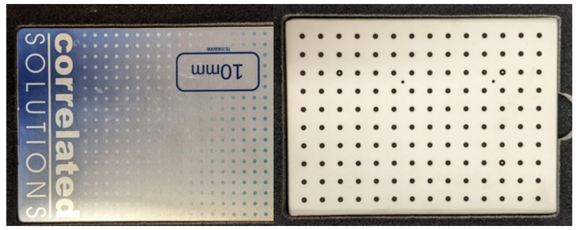

(a) Correlated Solutions 10 mm Aluminum Calibration Set

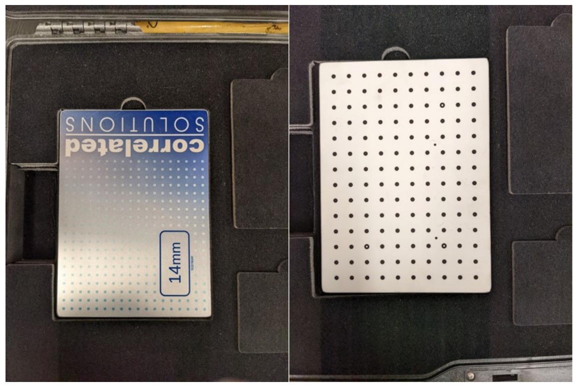

(b) Correlated Solutions 14 mm Aluminum Calibration Set

Figure 3.10: Aluminum Beam test specimens.

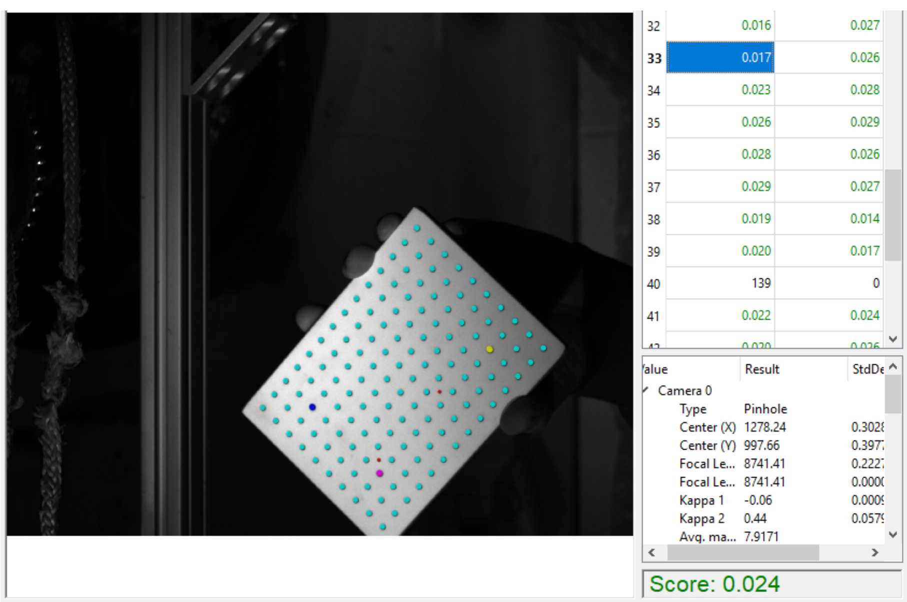

Figure 3.11: An ideal calibration with the error being less than 0.1

After calibrating the system, the specimen would be loaded in the test apparatus and placed in torsion shown in figure 3.12. Once the desired load was achieved, the researcher recorded the load and took the picture.

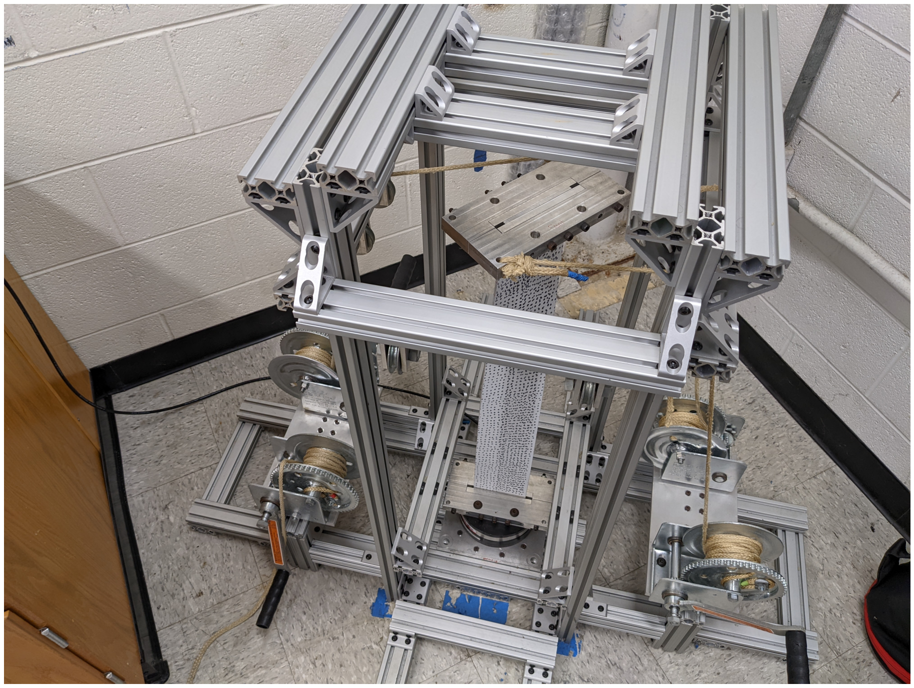

Figure 3.12: Aluminum Beam under torsion loading with winches 2 and 4 applying the load.

This process was repeated for 13 different torsional values starting from 0 Nm and wrenching to a maximum value of approximately 160 Nm. This was accomplished by approximately increasing the tension by every 2-clicks of the winches while increasing the torque by 10-20 Nm. When completed, proprietary software analyzed the strain and output the information into a MatLab readable file. This entire procedure, stated in this subsection, was conducted for distances of 5 ft, 6 ft, 8 ft, and 10 ft.

3.3 Theoretical Solution

The measured values were compared against thin wall approximation equation 3.4, where τ is the shear stress, *w* the width of the beam, *t* the thickness, and *Q* the torsion.

$$\tau = \frac{3Q}{wt^2} \tag{3.4}$$

The shear strain was calculated from equation 3.5, while the Shear Modulus was calculated from equation 3.6.

$$\epsilon_{xy} = \frac{\tau}{G} \tag{3.5}$$

$$G = \frac{E}{2(1+\nu)} \tag{3.6}$$

The material properties for the aluminum beam tested are shown table 3.4, where the Shear Modulus calculated from equation 3.6.

Table 3.4: Aluminium Beam Properties

Young's Modulus	69.9 GPa
Poisson's Ratio	0.33
Shear Modulus	51.42 GPa

3.4 Determining Accuracy

A MatLab script analyzed the data from Correlated Solution and computed the predicted based on equations 3.4, 3.5, and table 3.4. Once completed, the script then determined the relative error between the predicted and measured using equation 3.7.

$$percent\ error = \frac{(actual - predicted)}{predicted} \times 100 \tag{3.7}$$

All the strain measurements for each distance are shown in figures 3.13. For distances less than 6 ft, the measured strain is linear as expected for all materials within the elastic region. At distances of 6 ft or greater, the measured strain became less accurate against the predicted values. This is most noticeable in high strain values. This outcome was predicted due to the limitations with the specimen size. As the distance increased, so did the dot size, which reduced the available dots, hence, increasing the error. At high loads, the twisting of the beam made the cameras lose track of more dots which further exacerbated the error. Figures 3.13(c), 3.13(d), and 3.13(e) illustrate the effect of larger dots and high loading with lines that deviate further away from linear.

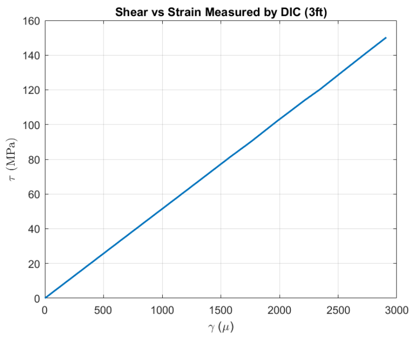

(a) DIC Apparatus 3ft

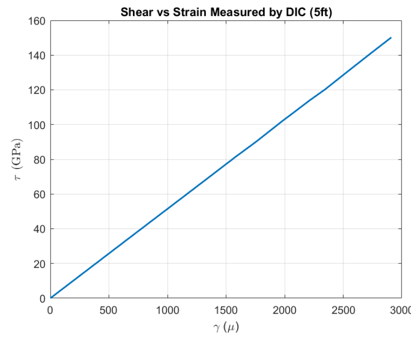

(b) DIC Apparatus 5ft

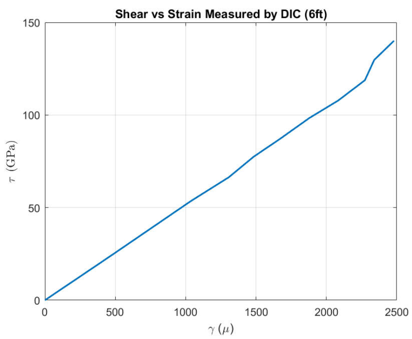

(c) DIC Apparatus 6ft

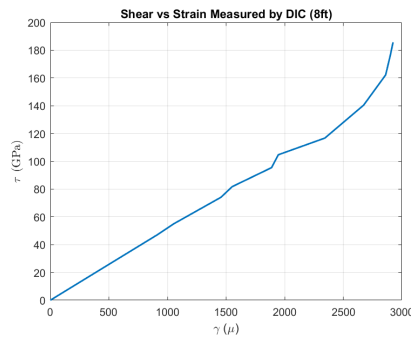

(d) DIC Apparatus 8ft

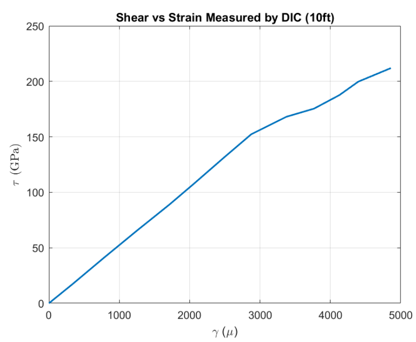

(e) DIC Apparatus 10ft

Figure 3.13: Shear vs Strain measured by DIC apparatus at different locations.

To provide further context, figure 3.14 shows the error with respect to predicted values. As mentioned before, the closer the cameras were to the specimen the higher the accuracy. Between 3 ft and 5 ft, the relative error between the predicted and actual were less than 1%. As the distanced increased, the relative error increased to between 1% and 2% for lower loads. At higher loads, this rapidly increased to between 9% and 18%. As mentioned before, a larger dot size was essential for the cameras to discern between the black dots and white background thus reducing the amount of dots and compounding the error. At higher loads, the displacement of the beam further depleted the available dots which escalated the relative error between the predicted and measured values.

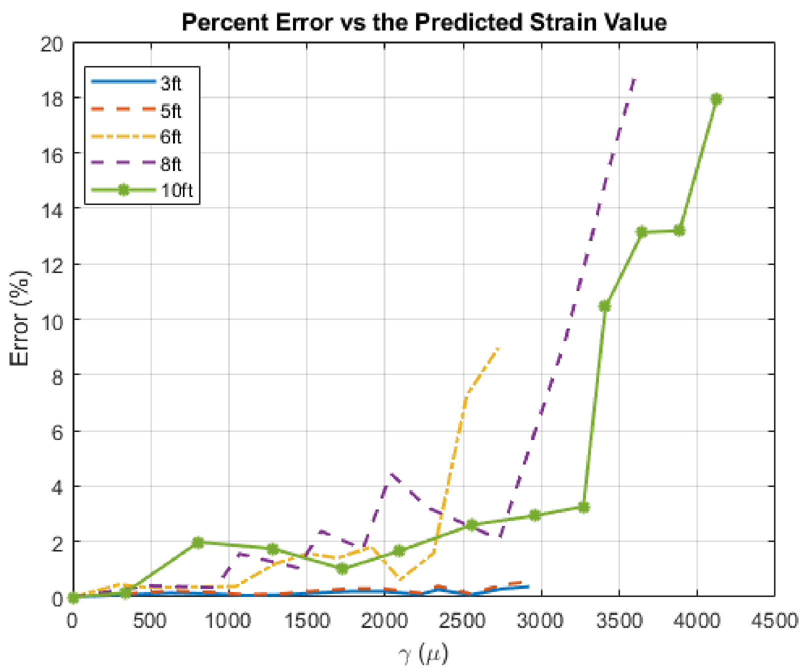

Figure 3.14: DIC Apparatus measured strain error between the predicted and actual.

The solution was further refined to between 5 and 7 pairs of cameras based on table 3.2 and figure 3.14. These solutions provided the best accuracy and closest working distance for the cost of the apparatus. Figure 3.15 illustrates the relationship between cost and relative error. The graph plots the average error for each distance and using table 3.2 determines the number of pairs of cameras associated with the distance. As the number pairs of cameras rose from 3 to 6 the average relative error drastically decreases from 6% to less than 1%. After 6 cameras, little change within the average error when compared to the cost to implement.

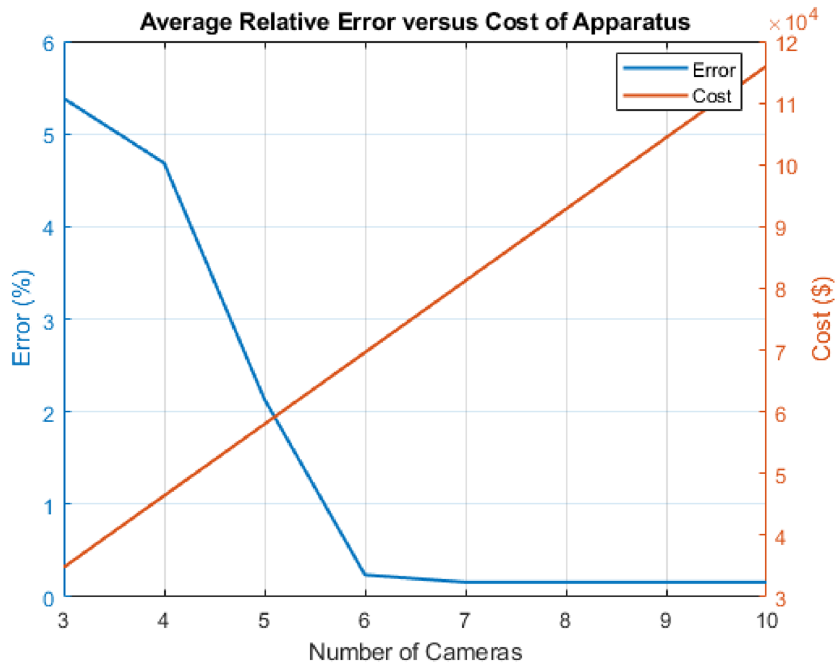

Figure 3.15: Average relative error per pair of cameras versus the cost for the number of cameras.

Chapter 4: Proposed Solution, Procedure, and Potential Induced Errors

Chapter 4 determines the proposed solution for a UH-60 blades based on cost, accuracy, and distance from specimen. The chapter provides an initial design and the initial set of equipment required to operate the DIC apparatus. Furthermore, it identifies the potential location for the equipment with respect to the blade. The chapter, finally, provides an initial set of procedures for operation, as well as identifying potential errors.

4.1 Proposed Solution

Table 4.1 provides the accuracy, working distance, and associated cost for the proposed 5 to 7 pairs of camera solutions. The study determined that a stationary 6 pair of 12.5 MP cameras with 20 mm lenses would be the best solution for an UH-60 helicopter blade. It was determined that the equipment could provide the required accuracy, while minimizing the working distance for the associated cost. It should be noted that the associated cost was only for the cameras and lenses. To effectively run the experiments, however, there should be an increase in the budget to around $100,000, accounting for software and other support equipment such as lighting, tripods, computers, etc.

Table 4.1: DIC Apparatus associated cost, working distances, field of view, and potential accuracy of the system based on the findings.

Number of Cameras (pairs)	Cost ($)	WD (ft)	FOV (ft)	Relative Error (%)
5	58000	6.02	5.3	2.13
6	69600	5.01	4.41	0.238
7	81200	4.30	3.78	0.159

4.2 Proposed Procedure

The proposed setup configuration for 6 pairs of cameras is illustrated in figures 4.1. The cameras are set 5 ft from the blade. At this distance, the cameras will be able to capture a field of view of 4.41 ft. Each pair of cameras will be separated by 4.41 ft as shown in figure 4.1. Six pairs of LED lighting similar to figure 3.7 will be placed behind each DIC tripod as depicted in figure 4.1. The placement and number of lighting sources will provide the required lighting to accurately measure the strain. Power sources close to the lights and cameras will provide the necessary power for both LED lights. Data cords run from each apparatus to a single DAQ device similar to figure 3.8. The DAQ device will operate the cameras and transfer the data to a single computer. According to Correlated Solutions, the single computer and DAQ device will be able to operate and collect information from all cameras.

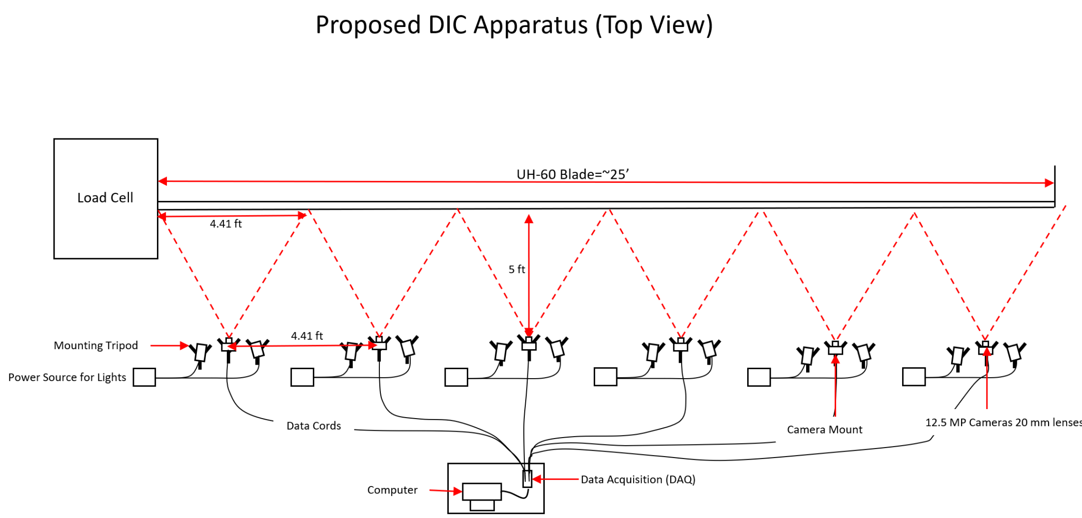

Figure 4.1: The proposed solution to map the strain for a UH-60 blade.

The proposed apparatus setup and chosen cameras are shown in figures 4.2 and 4.3. Each apparatus will have the mounting bracket set horizontally. The cameras will be placed at 22 in apart, based on experiments. The angle set for the cameras will be approximately 10° from the vertical axis. Data chords are attached to each camera and will be tied together prior to connecting to the DAQ device.

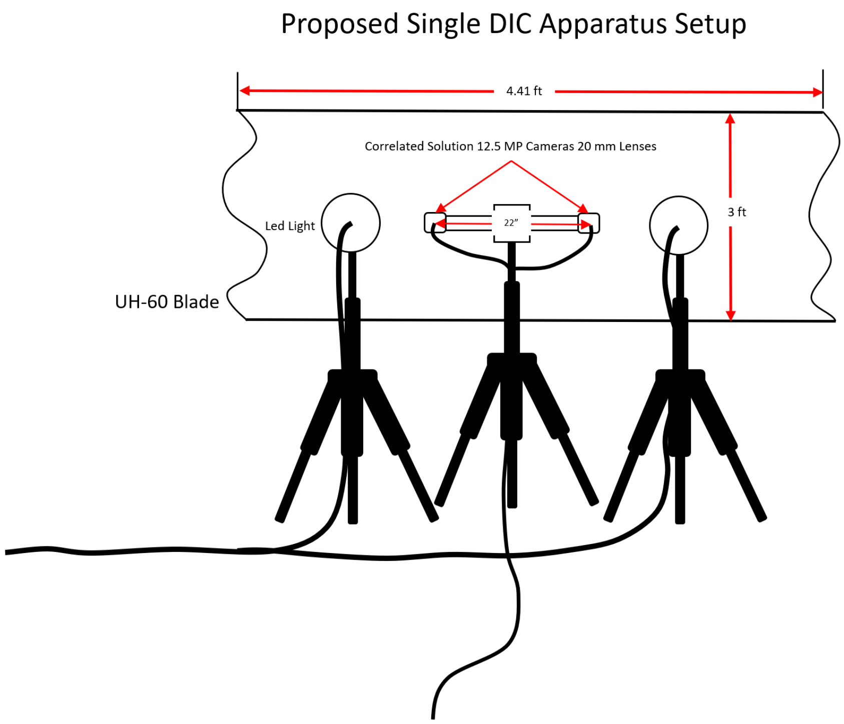

Figure 4.2: Proposed solution looking at the setup for one of the DIC apparatus.

Figure 4.3: Proposed Correlated Solution 12.5 MP camera. [5]

The UH-60 blade needs to have a 0.25 inch dot pattern painted, similar to figure 3.5, for the DIC to measure the strain values. This dot size is based on equation 4.1, where *SF* is the smallest feature, *SR* sensor resolution, and *FOV* the cameras field of view. Using table 3.1 for *SR* and table 4.1 for 6 pairs of cameras field of view, the smallest feature would need to be about 0.0303 inch. For this study the researcher increased the dot size to 0.25 inch. This increase provides higher resolution between white background and black dots.

$$SF = \frac{2 \times FOV}{SR} \tag{4.1}$$

A calibration test specimen like the one shown in figure 3.10 will be required to calibrate the cameras. Due to the unique design of the blade and test apparatus, it is recommended that a calibration blade be manufactured.

First, the tester will need to calibrate the system following the procedures outlined in subsection 3.2.6. If using a specially manufactured calibration blade, the specimen should be rotated and maneuvered to meet the required 50 calibration pictures. Once the system has been calibrated, the tester will apply the loads in the test procedures to capture the corresponding pictures. When completed, the tester uses the proprietary software to analyze the data and provide the strain values. This may need to be conducted in segments due to the inability of the software to analyze the entire blade from multiple sources. This requires the tester to add identifiers corresponding to the pair of cameras painted on the blade. If conducting further analysis on the data, Correlated Solution provides different formats for the data to be exported to the desire post analysis software.

4.3 Potential Errors

The most common errors occurs during the calibration of the cameras. These errors range from insufficient lighting to the calibration specimen being placed outside of the field of view for the cameras. All of these potential errors will lead to a low calibration score equal to or greater than 0.1. Figure 4.4 shows a poor calibration for the DIC cameras with an overall score of 4.114. Some of the errors are from poor hand placement covering calibration dots to moving the specimen out of the field of view for the cameras.

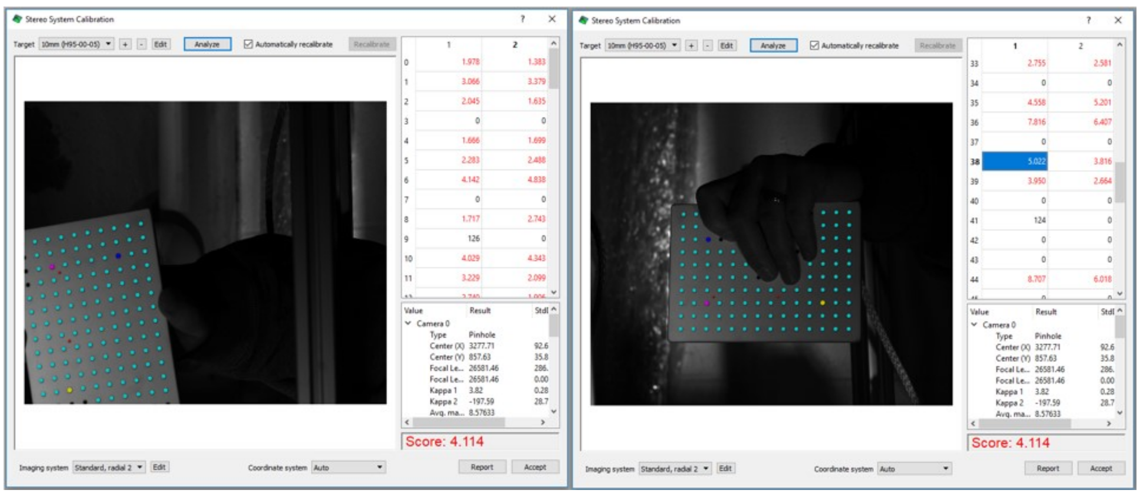

Figure 4.4: A poor stereo calibration of the system. Issues arose with hand placement, position of calibration set, and various other factors.

Another issue is the alignment of the the cameras. Shown in figure 4.5 this misalignment between the cameras causes one camera to lose focus of the calibration target before the other. In an ideal system the cameras should lose focus of the target at the same position or angle.

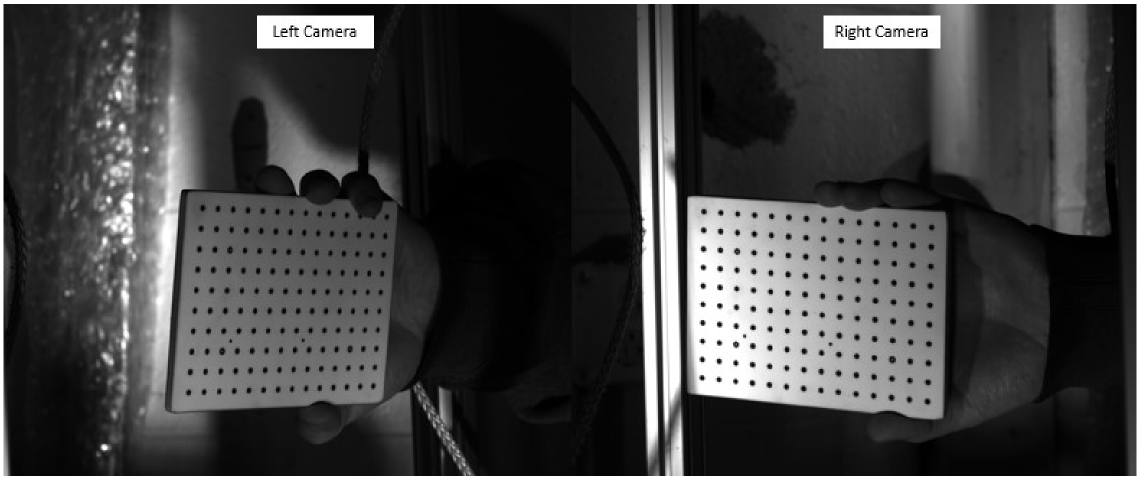

Figure 4.5: Cameras not set at the same angle. The left camera has the calibration set rotating at a higher angle than the right camera.

Lighting has a considerable impact on the calibration. During the initial calibration for the DIC Apparatus at 6 ft from the specimen, insufficient lighting prevented the system calibrating the cameras. This is shown in figure 4.6 with an ideal lighting and the lighting present at 6 ft test run. The poor lighting of the system would not calibrate the cameras, because the software was unable to recognize the calibration device. Further re-positioning and experiments produced the required lighting for the system to calibrate.

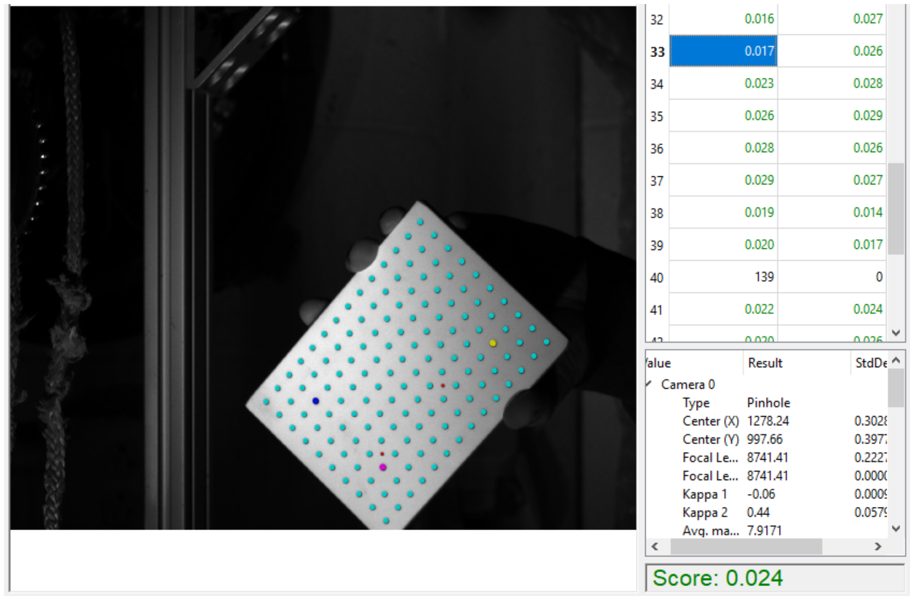

(a) Ideal lighting for calibration and the low error.

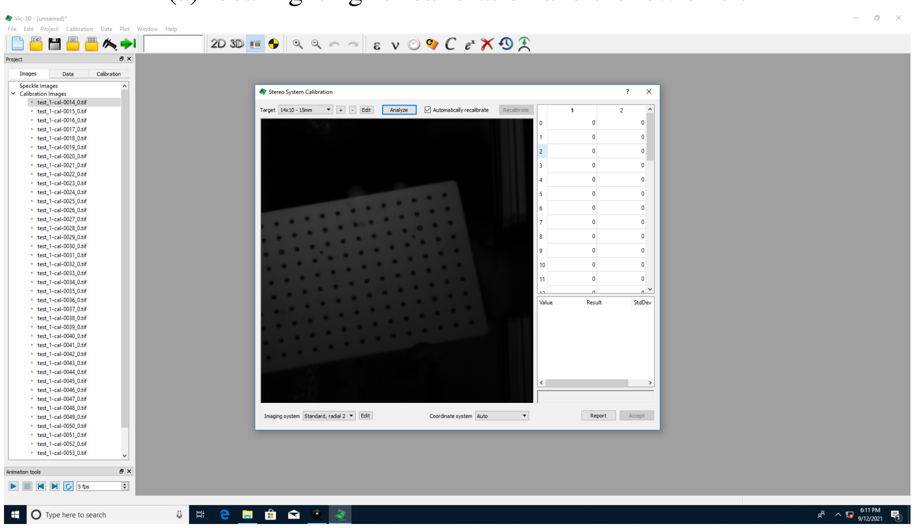

(b) Poor lighting for calibration and the effects.

Figure 4.6: Lighting effects on the calibration of DIC cameras.

Another user induced error is shifting any piece of equipment during the test. During the test, the light source shifted from the optimal position as shown in figure 4.7.

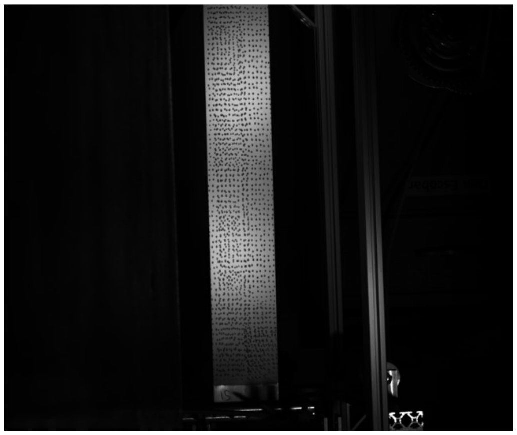

(a) Strain test with required lighting.

(b) Strain test with poor lighting.

Figure 4.7: Strain test at 10 ft with DIC Apparatus and the effects of lighting shifting.

The cameras were unable to distinguish the dots, thus increasing error within the strain analysis. Figure 4.8 shows this as a plot of the required and poor lighting with the latter line shifting away from linear.

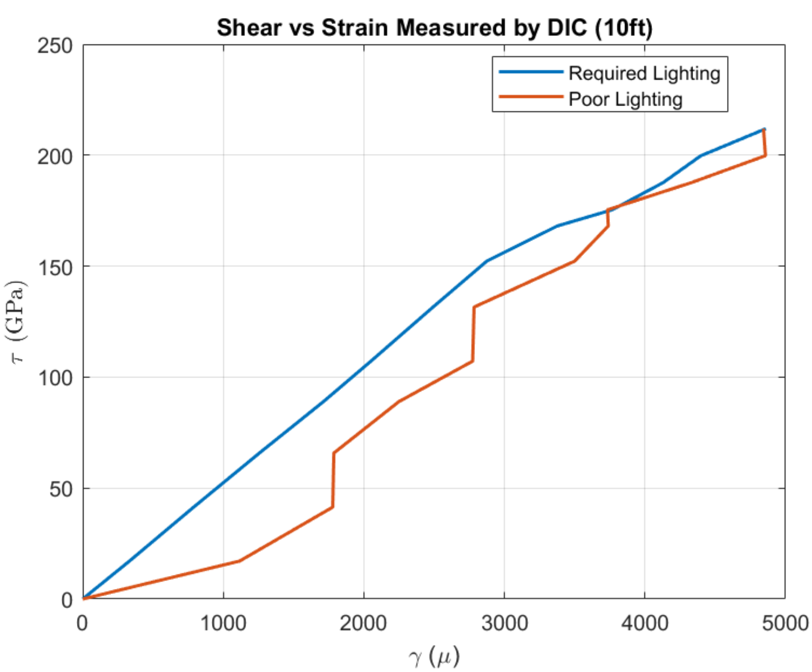

Figure 4.8: Strain versus load with ideal lighting and suboptimal lighting.

Final induced error is the size of the specimen compared to the surroundings. Figure

4.9 provides Correlated Solutions suggested sample size compared to substandard sizes.

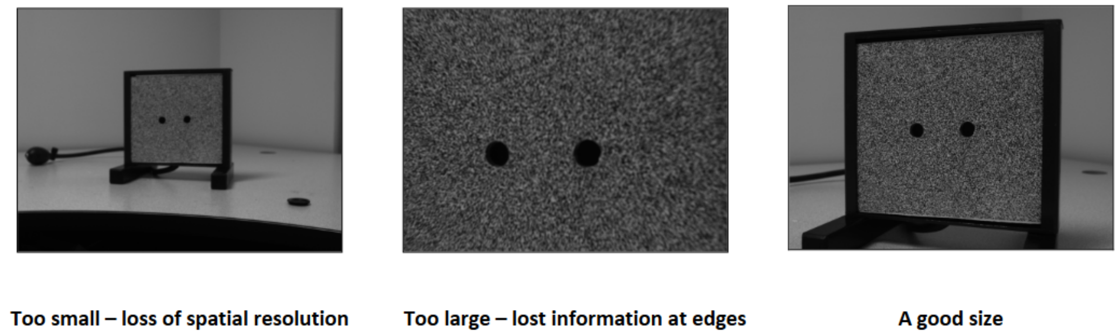

Figure 4.9: Correlated Solutions too small, too large, and ideal sample size for DIC. [6]

If the sample is too small relative to the surroundings, then cameras lack the resolution to determine strain. This issue presented in any distance greater than 6 ft from the test apparatus. Figure 4.10 shows the discrepancy with the left figure showing the DIC apparatus at 3 ft compared to 6 ft. When the DIC apparatus is at 3 ft specimen fills most of the picture, where as at 6 ft it does not. Thus, increasing the relative error as shown in figure 3.14.

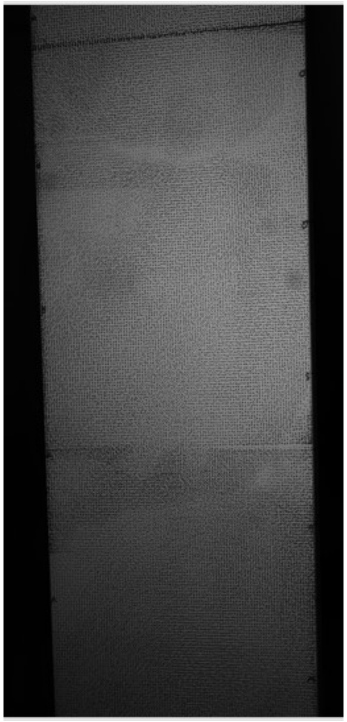

(a) Image captured when DIC Apparatus was at 3 ft.

(b) Image captured when DIC Apparatus was at 6 ft.

Figure 4.10: The sample size versus the distance of the DIC Apparatus.

Chapter 5: Conclusion

Chapter 5 summarizes the entire study by first reviewing the information discussed in the previous chapters. Then the chapter provides a summary of the findings for chapters 2 and 3. Chapter 5 concludes with the results discussed in chapter 4 and the final solution determined from this study. Lastly, some suggestions for further research is discussed.

5.1 Summary

The purpose of the study was to determine effectiveness for a DIC apparatus to measure sectional stiffness properties of full-scale rotor blades with high accuracy as well as the ideal system to conduct the measurements. This study reviewed comparable tests, such as the TRACT and ELTSAR, to determine the effectiveness for a DIC apparatus at facilities with the necessary load cells, such as Fort Eustis. Moreover, to determine the ideal system, this study evaluated two initial designs, the gantry and stationary systems. Using different types of evaluation matrices and considering the pros and cons of each system, the stationary system was evaluated as the ideal system to measure strain. Through experimentation and calculation, a 6 pair of 12.5 MP cameras with 20 mm lenses set at approximately 5 ft from the helicopter blade were determine to provide the ideal solution to analyze the data. This provided an accuracy to measure strain within less than 1%.

5.2 Final Result

In conclusion, the total cost for the solution would be approximately $100,000 which included the required cameras, lenses, support equipment (lighting, data processors, stands, etc), computers, and software to operate the system. To sum up, this study concluded that a DIC apparatus would be able to measuring the strain with a high accuracy.

5.3 Further Studies

While this study was able to determine the effectiveness of a DIC apparatus, the study was unable to construct a full scale apparatus and measure strains on a helicopter blade. Further studies will be required using full scale blades and the required load cells to determine the ideal solution. Moreover, for most accurate results, tests should be conducted at designated facilities, such as Fort Eustis. Lastly, while this study proposed a potential cost for the test, further analysis for finalized total cost, required equipment, and procedures for such an apparatus is recommended.

Bibliography

[1] Justin Littell. Experimental Photogrammetric Techniques Used on Five Full-Scale Aircraft Crash Tests. `https://ntrs.nasa.gov/search.jsp?R=20160005896`, 2017.

[2] Martin Annett and Justin Little. Overview of the Transport Rotorcraft Airframe Crash Testbed (TRACT) Full Scale Crash Test. `https://ntrs.nasa.gov/archive/nasa/casi.ntrs.nasa.gov/20160006501.pdf`, 2013.

[3] Timothy S. Davis. Six axis testing machine, 2020.

[4] Correlated Solutions. *Minimizing Noise and Bias in 3D DIC*. Correlated Solutions Inc., 2013.

[5] Correlated Solutions. *Product Catalog*. Correlated Solutions Inc., Irmo, SC, 2018.

[6] Correlated Solutions. *VIC-3D 9 Setup Procedures*. Correlated Solutions Inc., Irmo, SC, 2021.

[7] Tyler Mel Sinotte. *A Strain-Based Eexperimental Methodology for Measuring Sectional Stiffness Properties of Composite Blades*. PhD thesis, University of Maryland, College Park, MD, 2020.

[8] Correlated Solutions. *VIC-3D SOFTWARE MANUAL Version 9.4*. Correlated Solutions Inc., Irmo, SC, 2021.